Imaging With Known Pointing Errors

M.A. Holdaway
National Radio Astronomy Observatory
Socorro, NM 87801

April 1, 1993

1 Introduction

Radio interferometers are often used at high frequencies where the pointing errors are no longer a small fraction of the primary beam. When the observed source is small compared to the primary beam, the resulting amplitude errors can be removed by self-calibration. However, if the source size is comparable to the primary beam or larger, pointing errors will produce errors in the visibilities which do not factor into a single gain term. Until now, the best that could be done with an interferometer was to perform pointing measurements to "peak up" the antennas prior to the observing program, or to flag visibilities which contained antennas which were found to be grossly mispointed.

Since the MMA will be imaging large objects a good deal of the time, a tight pointing error specification of 1″ has been placed on the MMA's elements. Some people have criticized this design specification on the grounds that it would be difficult and expensive to obtain 1″ pointing for 40 antennas. Even with 1″ rms pointing errors, the MMA mosaic images would have a dynamic range of less than 1000:1 and a fidelity of less than 20:1 for observations of bright sources at 230 GHz (Holdaway, 1990). It should be emphasized that similar dynamic range and image fidelity limitations occur when a large single dish is used to measure total power instead of the interferometer elements used in the homogeneous array scheme. While 1000:1 dynamic range and 20:1 image fidelity will not compromise the scientific objectives of the majority of mosaicing projects performed by the MMA, there are experiments, such as the continuum mosaicing of Cygnus A, which would be compromised. In order to get the most out of the instrument as designed with 1″ pointing errors, new algorithms must be developed to determine and correct pointing errors. We present here an algorithm which can take corrupted visibilities and known pointing errors as a function of time and antenna number and invert them to yield high quality images.

2 Determining Pointing Errors

Generally, the pointing errors of the elements in an interferometric array cannot be determined to arbitrary precision. Attempts may be made to measure the pointing with hardware or with observations of pointing calibrators, but the pointing will change with time as the antennas

travel through the pointing model's phase space and as the antenna structure deforms due to gravity, thermal effects, and wind loading. If the effects of the pointing errors limit the quality of the resulting image, it is likely that there is enough signal to determine the pointing parameters through *pointing self-calibration*, which has not yet been developed. Pointing self-calibration requires the evaluation of the partial derivative of each visibility with respect to the pointing of each element's pointing position, which requires the computational equivalent of two direct Fourier sums for each visibility. Pointing self-calibration may be the subject of a future MMA Memo.

3 Imaging

For astronomical sources of large angular size, there is no way to correct the visibilities for mispointing. In other words, the pointing errors do not factor into antenna or baseline gains. Hence, it will not be possible to use a direct method such as inversion of all of the data followed by deconvolution. The Maximum Entropy Method (MEM) lends itself to difficult inverse problems, as it is driven to a solution by the difference between the data visibilities and the model visibilities. Hence, if it is possible to calculate model visibilities from a model image and pointing errors for each antenna as a function of time, there is a MEM-based algorithm which will produce an image.

In the following discussions, I refer to the old mosaic algorithm as *standard mosaic*, and the new algorithm presented here as *pointing mosaic*. Without pointing errors, the gradient of χ^2 is calculated in the following manner (Cornwell, 1989):

- Initialize $\nabla\chi^2$ image to zero.
- Loop over pointings.
- Apply appropriate primary beam pattern to current estimate of the ME image.
- FFT beam applied image and degrid to obtain the predicted visibility $\hat{V}$.
- Accumulate $\chi^2 = \sum |V - \hat{V}|^2/\sigma^2$.
- Form residual visibility $V - \hat{V}$.
- Grid and FFT residual visibility to image plane.
- Apply primary beam pattern to result.
- Add to $\nabla\chi^2$ image.
- End loop over pointings
- Use $\nabla\chi^2$ image to change the current ME image to obtain the next iteration ME image.
- Return to step 1 until convergence.

The entropy measure of the current ME image is also involved in determining how to change the ME image.

In the presence of pointing errors, there is still a Fourier transform relationship between the sky brightness multiplied by the two antennas' voltage patterns and each visibility sample, but because each antenna's voltage pattern is centered at a different point on the sky, the quantity being Fourier transformed is different for each antenna:

$$\hat{V}_{1,2}(\mathbf{u}) = \int \hat{I}(\mathbf{x}) E_1(\mathbf{x} - \mathbf{x}_{1p}) E_2^*(\mathbf{x} - \mathbf{x}_{2p}) e^{j2\pi \mathbf{u}.\mathbf{x}} \, d\mathbf{x}, \tag{1}$$

where $\mathbf{x}$ is the sky coordinate, $\mathbf{x}_{1p}$ is the pointing center of antenna 1, E_1 is the voltage pattern of antenna 1, $\hat{I}(\mathbf{x})$ is the model brightness distribution, and $\hat{V}_{1,2}$ is the model visibility between antennas 1 and 2. The optimal way to calculate the model visibility from the model image is by a direct Fourier sum for each individual visibility sample. Hence, the standard mosaic procedure described above is modified in the following manner:

- Initialize $\nabla\chi^2$ image to zero.
- Loop over pointings, visibilities *one at a time!*
- Apply the voltage patterns appropriate to the two antennas and their pointing errors to current estimate of the ME image (Equation 1).
- Fourier transform to obtain one predicted visibility $\hat{V}$.
- Accumulate $\chi^2 = \sum |V - \hat{V}|^2/\sigma^2$.
- Form residual visibility $V - \hat{V}$.
- Fourier transform *of one visibility* to image plane.
- Multiply result by voltage patterns of the appropriate antennas centered on the appropriate pointing positions.
- Add to $\nabla\chi^2$ image.
- End loop over visibilities, pointings.
- Use $\nabla\chi^2$ image to change the current ME image to obtain the next iteration ME image.
- Return to step 1 until convergence.

In the standard mosaic, all visibilities for a single pointing can be treated at once. Since the visibilities in the pointing-mosaic case must be treated individually, each visibility sample behaves as if it were taken from a different pointing center with a unique primary beam.

4 Simulations

To demonstrate the success of mosaicing with known pointing errors, I have performed a few toy simulations. The simulations are not intended to represent any actual measurements with existing or planned instruments, but they show clearly that if the pointing errors are known perfectly, the resulting images will be of the same quality as if there were no pointing errors at all. Stated more realistically, in the absence of other types of errors, the resulting image will be limited by the *residual* pointing errors, or the difference between the true pointing errors and the alleged pointing errors.

The toy simulations used a 32 x 32, 5″ pixel model image which is derived from the standard M31 optical HII region image used in previous MMA imaging work. The simulated array consisted of 7 antennas, each 7.5 m in diameter, arranged in a circle 20 m in diameter. The shortest spacing was about 8 m, the longest about 20 m. The antennas made total power and interferometric measurements simultaneously. Nine pointings on the model source were made with $\lambda/2D$ separation, or 17.″9 at 230 GHz. The total observing time was 1 hour and each pointing was observed for four integrations of 100 seconds, separated in time to obtain better (u, v) coverage. Systematic and random pointing errors with an rms value of about 17″ (see Holdaway, 1990 for the pointing error model) were used to generate one dataset, and no pointing errors were used for a control dataset. The pointing errors as a function of time and antenna number were recorded in a pointing database attached to the mosaic database. In general, no two antennas have the same pointing at any given time. Note that these simulations were particularly severe with pointing errors comparable to the HWHP primary beam. (Since the (u, v) coverage was not great, I wanted to be sure the effects of the pointing errors dominated the image.) A large loss of sensitivity would result with such large pointing errors as the overlap in the voltage patterns of any two antennas would be much less than if the antennas were correctly pointed. This effect is not seen in the simulations since no thermal noise was added to the visibilities, and the lower values of the visibilities are correctly accounted for in the imaging process. The simulated datasets were imaged with both the nonlinear mosaic algorithm (Cornwell, 1989) and with pointing mosaic.

In the control imaging with no pointing errors, the standard mosaic algorithm and the pointing mosaic algorithm produced very similar images. The peak image flux divided by the rms of the difference between the two images was 30000. The cause of this difference is still being investigated. For all practical purposes, we can say that the pointing mosaic gives the same answer as standard mosaic. The convolved model image, the sensitivity pattern, and the control image are shown in Figures 1 through 3

When the dataset with large pointing errors was imaged with the standard mosaic algorithm, the results were quite poor (Figure 4). The best thing that can be said about this image is that the total flux is within 20% of the correct value. However, when the same corrupted data are imaged with pointing mosaic and the pointing errors are compensated for in the imaging process, an excellent image results (Figure 5). This image is different from the image with no pointing errors because the pointing errors have broadened the sensitivity pattern on the sky. The pointing-mosaic image is of comparable quality to the standard mosaic image without

pointing errors. More extensive simulations and error analysis will probably be made in the future.

5 Computing Cost

The pointing mosaic simulations reported above entailed very small image sizes and a very small number of visibilities, and yet took 44 minutes of CPU time on a Sun Sparcstation IPX. Since the pointing mosaic program is dominated by the direct Fourier sum, the cost is independent of the number of pointings, linear with the number of visibilities, and linear with the number of pixels in the part of the image which is covered by the primary beam. Hence, we can use the size of our problem to estimate the required CPU time for larger problems. The number of pixels required for each DFT in an array of maximum baseline B and dish diameter D will be approximately

$$N_{pix} = \pi(2.5B_{max}/D)^2. \tag{2}$$

Our simulations were performed with a primary beam model which extended to the second null, so our simulations would have run a factor of 4 faster if we had modeled the primary beam only out to the first null, as is often used in reconstruction. From the above arguments, we see that the time required to perform the pointing mosaic will be about

$$t = 0.0015N_{vis}(B_{max}/D)^2 \tag{3}$$

in Sparc IPX CPU minutes. We estimate t for a number of instruments:

- For a small millimeter interferometer (5-element) observations in three configurations, integration times of 30 seconds, and 8 hour tracks (9600 visibilities) with dish diameter of 10 m and longest baseline of 60 m, we would expect the computing time to be about 8 hours of Sparc IPX CPU time.
- For GMRT observations in the compact configuration (14 elements) with integration times of 30 seconds and 1 hour tracks (10920 visibilities) with a dish diameter of 45 m and a maximum spacing of 1200 m, the required Sparc IPX CPU time is about 200 hours. The algorithm lends itself to parallel machines with powerful processors, so GMRT's parallel computers may make this feasible.
- For the MMA operating for only 1 hour with 30 second integrations in its compact 70 m array, the required computing time is 20 hours. Assuming that the speed of the computer on your desk will double every 18 months until 2001, the target date for full MMA operations, the required time to image the 1 hour MMA observations with pointing mosaic will be well under an hour.
- For VLA observations in the D array with 30 second integration time and 1 hour tracks (42120 visibilities), the required Sparc IPX CPU time is about 1700 hours, which is clearly not possible. The large time required is due to the large number of resolution elements

in the VLA's primary beam. The problem becomes even more intractable for the more extended configurations of the VLA. However, the VLA stands to gain more through the possible use of grouped FFTs rather than the direct Fourier sum (see below).

For the time being, the current algorithm may be sufficient for the existing millimeter interferometers: it is faster than real time observing for continuum, but slower than real time observing for spectral line. It should be trivial to alter the algorithm such that the full DFT machinery is used only for certain time ranges strategically placed around sunrise and sunset, visibilities taken outside these timeranges being processed with an FFT.

It may be possible to take shortcuts in pointing mosaic. For example, if we had a very large number of antennas N, and we "quantized" the pointing errors in space and time such that there were only M values of pointing errors, we would achieve some improvement in the image quality at some computational cost. FFTs would be performed for the image multiplied by the voltage pattern centered on pointing i and by the voltage pattern centered on pointing j, for all possible pairs of i and j, resulting in $M(M-1)/2+M$ times as many FFTs as the standard mosaic program. For example, with $M=4$, 10 times as many FFTs would be required. Assuming the dynamic range is inversely proportional to the rms pointing error, as predicted by Cornwell, Holdaway, and Uson (1992) and as verified in simulations by Holdaway (1990), assuming four possible values of the pointing error would reduce the rms pointing error by a factor of about 0.6, increasing the dynamic range by a factor of 1.7. It is clear that increasing M much beyond 4 will not result in any savings over the DFT approach as the number of FFTs increases like M^2. However, if each pointing error solution is applicable for several integration times, then each FFT (one for each pair of quantized pointing errors) can be used for more visibilities, each of which would require a DFT in the exact solution.

Since the terms required in $\nabla\chi^2$ are similar to the terms required for the partial of χ^2 with respect to the pointing error, which is required for pointing self-calibration, it should be possible to implement the pointing error determination inside the imaging program. When the image begins to suffer from the effects of pointing errors, the image is used as a model for pointing self-calibration. The image is then used as the starting model for several more iterations of imaging, until the effects of residual pointing errors are again limiting the image. Such a scheme would save a lot of computer time over the current approach to deconvolution and self-calibration in which both programs are run anew each time.

6 Summary

The mosaic algorithm has been extended to properly treat known pointing errors in the imaging of radio interferometric data. Images produced by the new algorithm should have an error level dictated by the level of the residual pointing errors (ie, the difference between the true pointing errors and the pointing errors used in the algorithm). This new algorithm is computationally expensive, but should be feasible for existing small millimeter wavelength interferometers, for the GMRT with parallel processing, and for the MMA with expected increases in computer performance. The algorithm cannot be applied to VLA data any time soon. This algorithm will also work for single dish data and single pointing interferometer data. The algorithm can easily be extended to cope with antennas with different (known) voltage patterns.

7 References

1. Cornwell, T.J., and Evans, K.F., 1985, Astron. Astrophys., **143**, 77–83.
2. Cornwell T.J., 1988, Astron. Astrophys. **202**, 316–321
3. Cornwell, T.J., 1989, in *Synthesis Imaging in Radio Astronomy*, ed. Perley, Schwab, and Bridle, Astronomical Society of the Pacific, 277–286
4. Cornwell, T.J., Holdaway, M.A., and Uson, J. 1993, accepted to Atron. Astrophys.
5. Holdaway, M.A., 1990, "Imaging Characteristics of a Homogeneous Millimeter Array", MMA Memo 61.

Figure 1: Model brightness distribution used in the simulations, convolved with the synthesized beam.

Figure 2: Sensitivity on the sky for a 9 pointing mosaic.

Figure 3: Image resulting from mosaicing the error-free data with either the mosaic or the pointing mosaic algorithms.

Figure 4: Image resulting from the standard mosaic's attempt to image data with very large (~HWHM primary beam) pointing errors.

Figure 5: Image resulting from the pointing mosaic algorithm applied to the data with very large pointing errors.

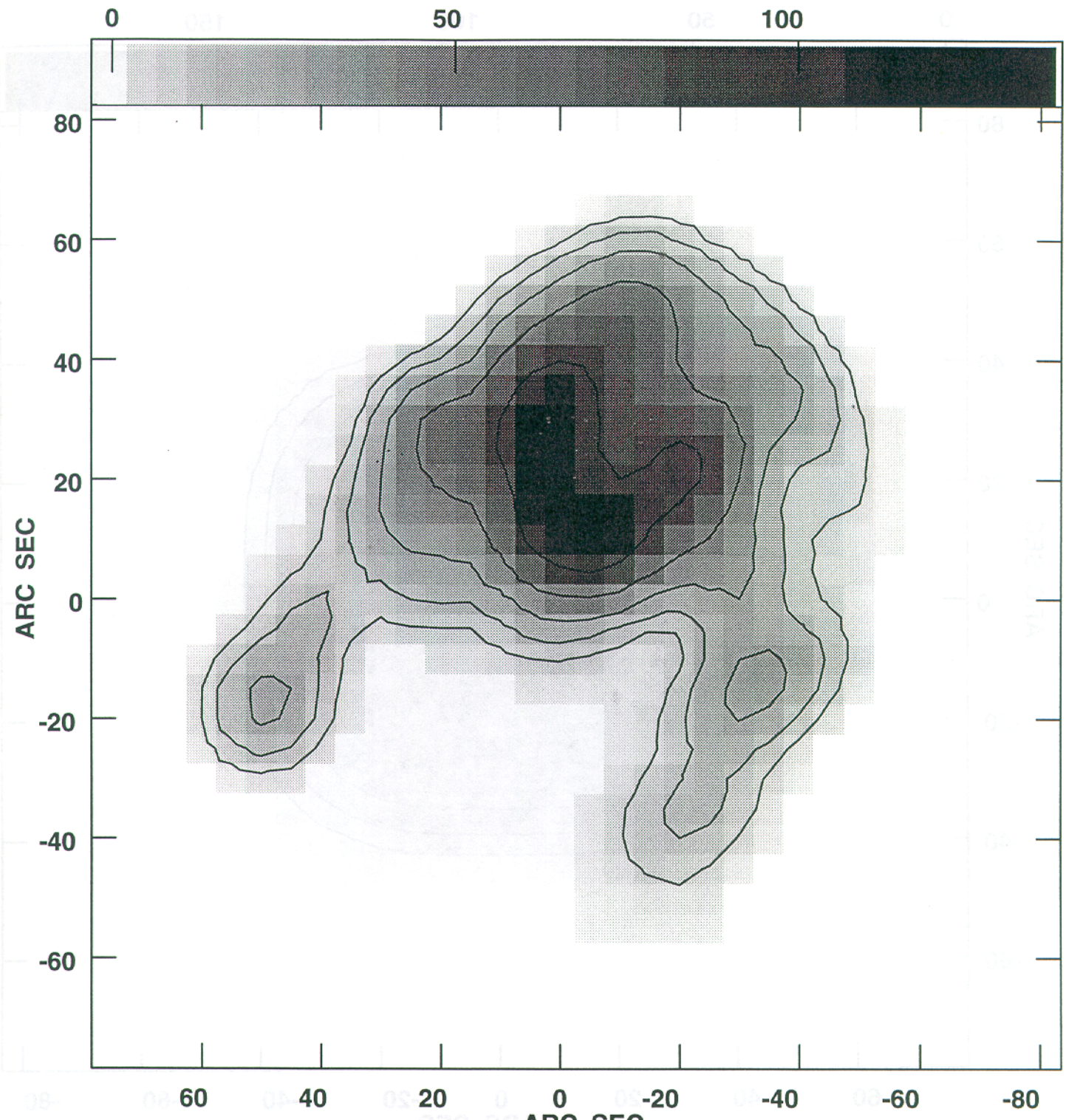
Plot file version 1 created 12-AUG-1992 18:45:15
MMA-TEST M31MOD.SMOOTH.1
0
50
100
80
60
40
20
0
-20
-40
-60
ARC SEC
60
40
20
0
-20
-40
-60
-80
ARC SEC
Center at RA 00 00 0.000 DEC 35 00 0.00
Grey scale flux range= 0.0 135.1 JY/BEAM
Peak contour flux = 1.3515E+02 JY/BEAM
Levs = 1.3515E+00 * (4.000, 8.000, 16.00,
32.00, 64.00)

– Figure 1 –

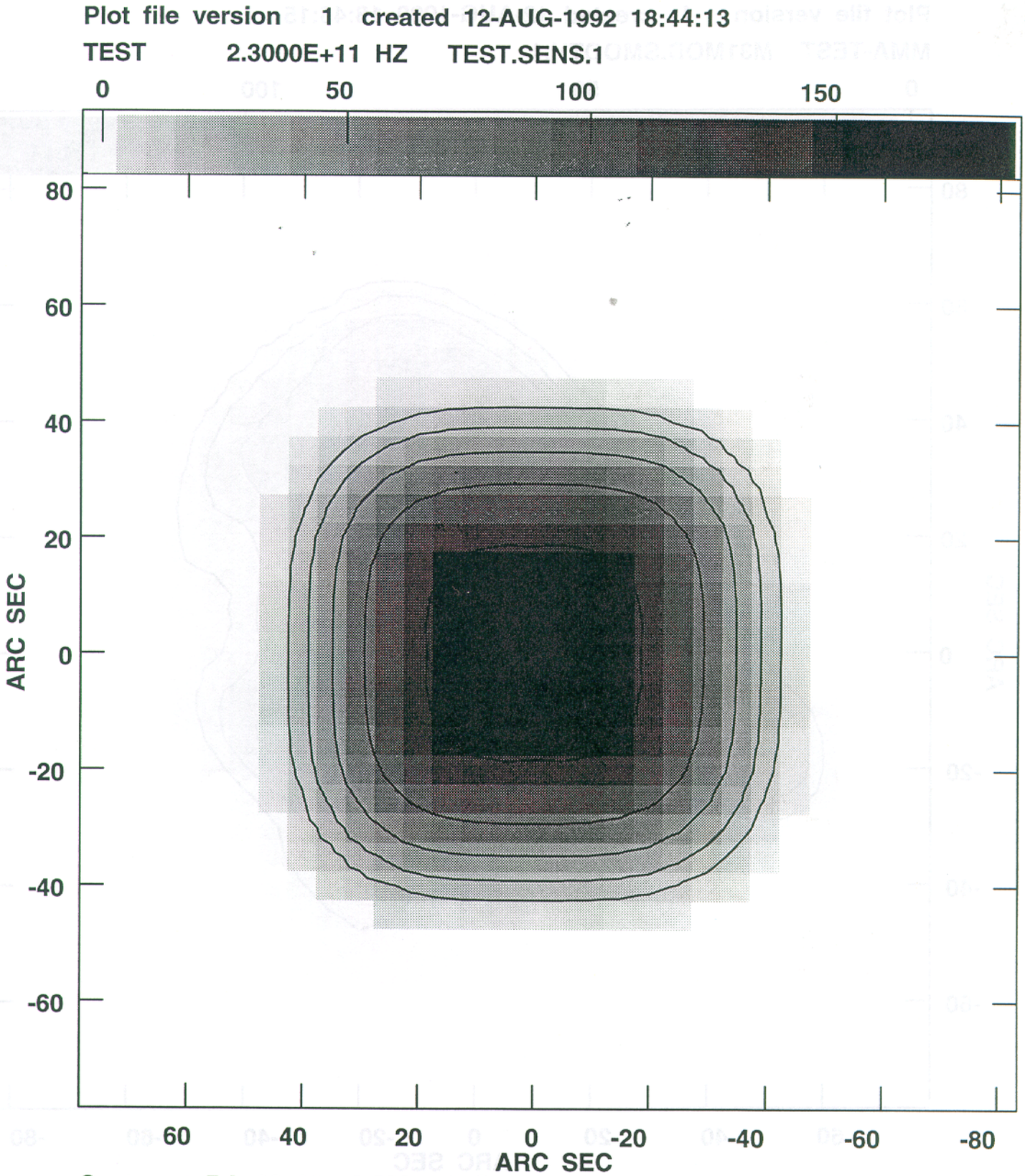

Center at RA 00 00 0.000 DEC 10 00 0.00
Grey scale flux range= 0.0 183.7 WEIGHT
Peak contour flux = 1.8370E+02 WEIGHT
Levs = 1.8370E+00 * (5.000, 10.00, 20.00,
40.00, 80.00)

— Figure 2 —

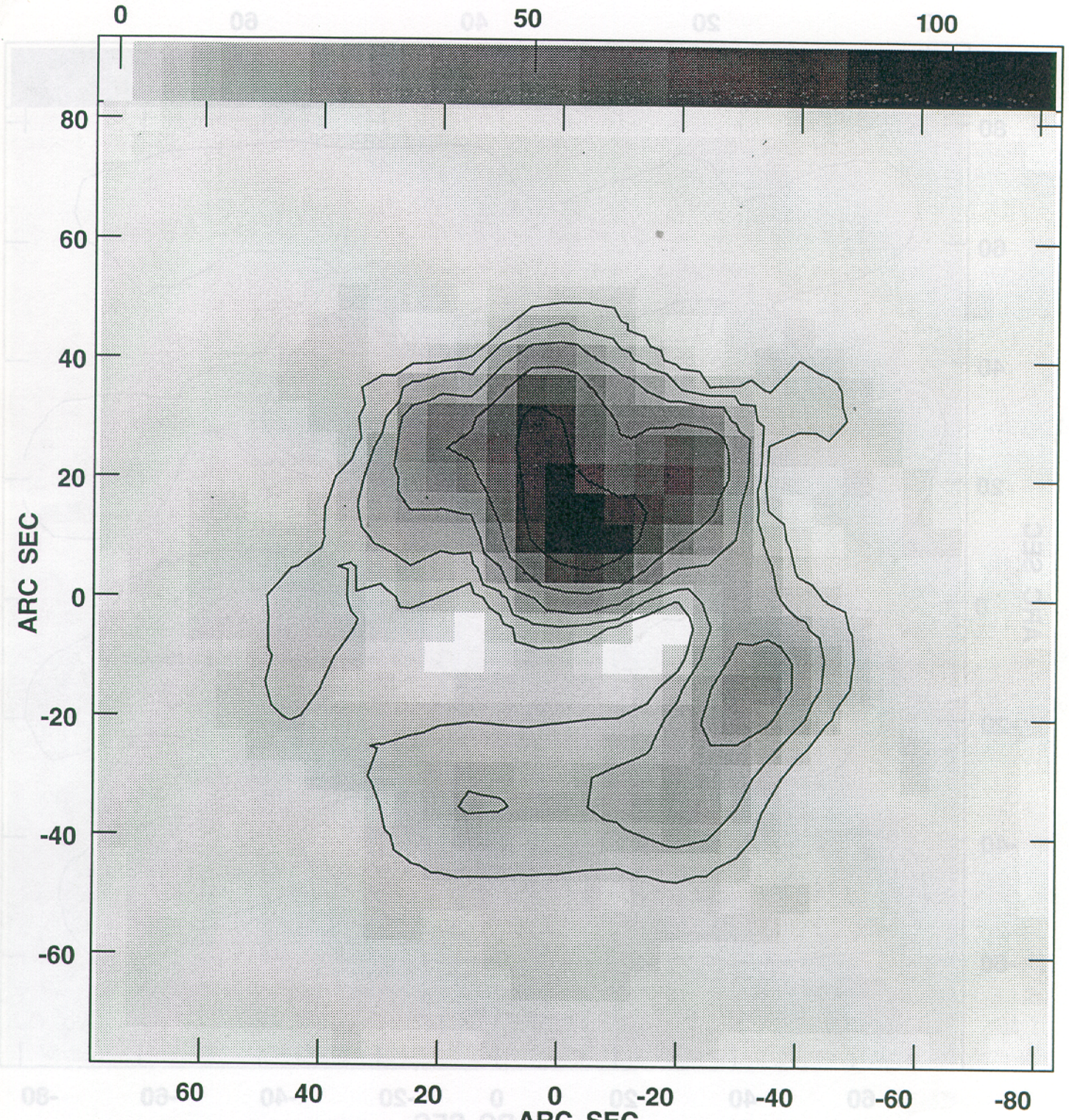
Plot file version 1 created 12-AUG-1992 18:45:45
TEST 2.3000E+11 HZ TEST.CVM.1
0
50
100
80
60
40
20
0
-20
-40
-60
ARC SEC
60
40
20
0
-20
-40
-60
-80
ARC SEC
Center at RA 00 00 0.000 DEC 10 00 0.00
Grey scale flux range= -0.2 110.7 JY/BEAM
Peak contour flux = 1.1073E+02 JY/BEAM
Levs = 1.1073E+00 * (4.000, 8.000, 16.00,
32.00, 64.00)

— Figure 3 —

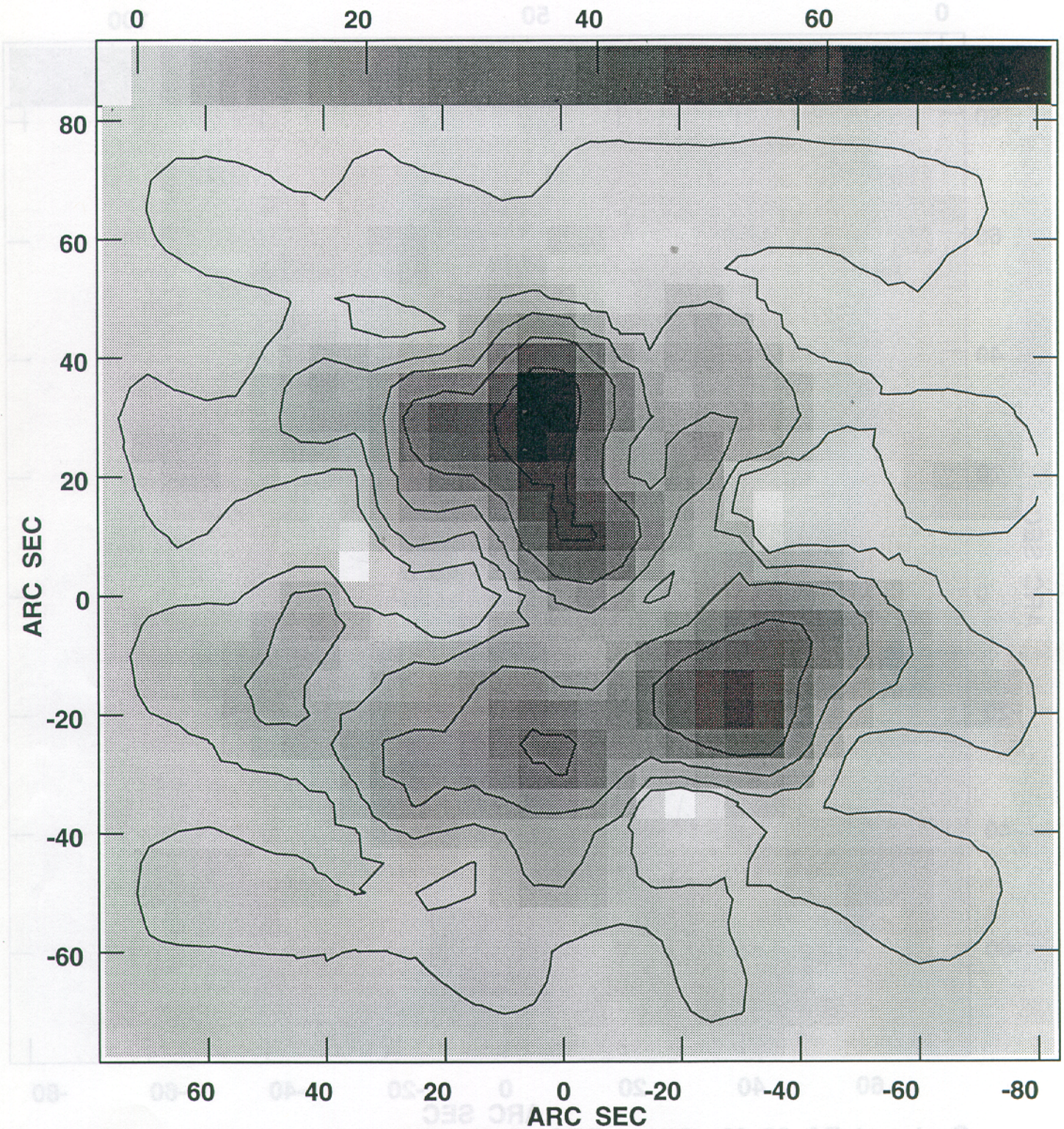

Center at RA 00 00 0.000 DEC 10 00 0.00
Grey scale flux range= -1.8 78.1 JY/BEAM
Peak contour flux = 7.8053E+01 JY/BEAM
Levs = 7.8053E-01 * (4.000, 8.000, 16.00,
32.00, 64.00)

— Figure 4 —

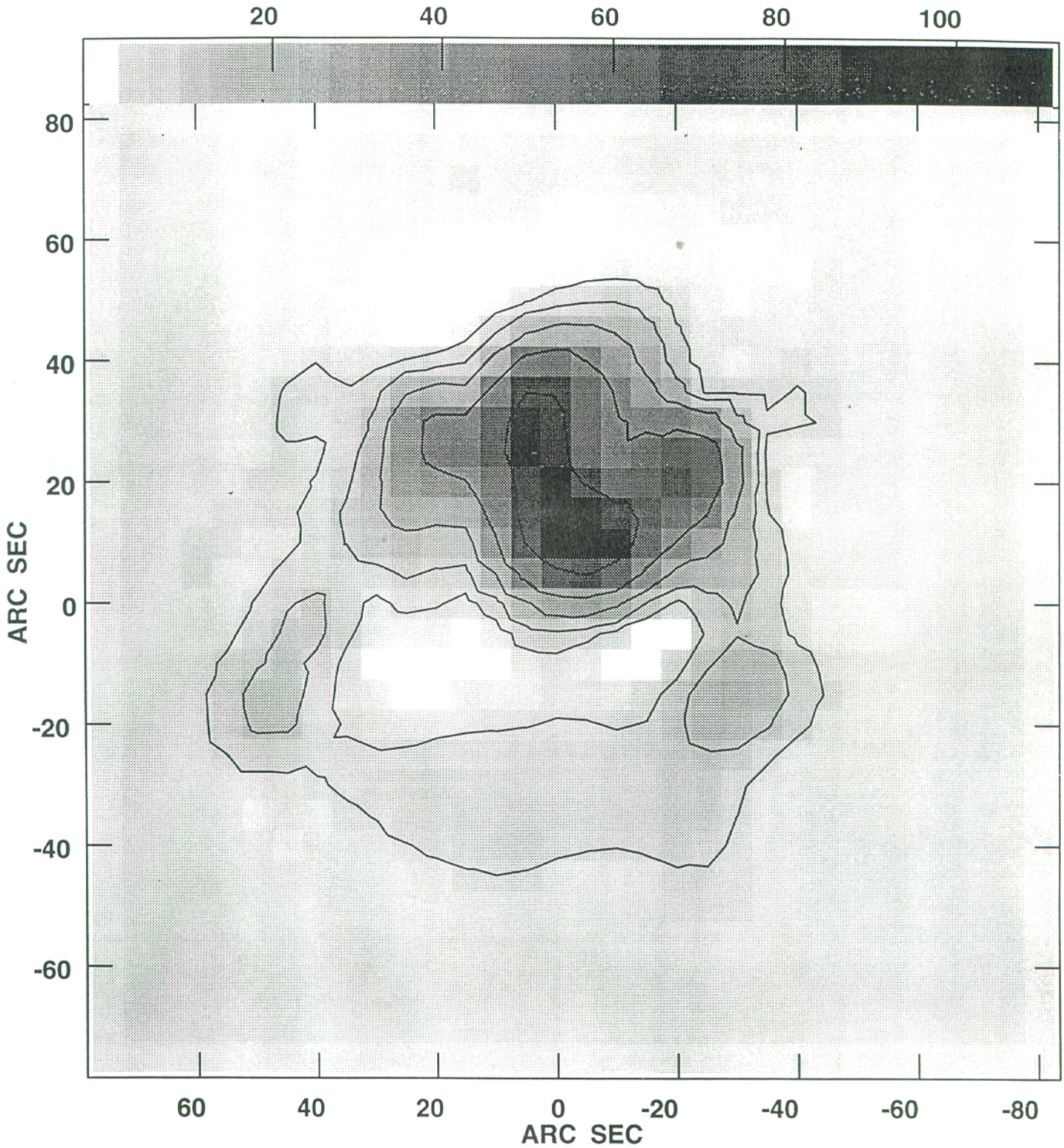
Plot file version 1 created 12-AUG-1992 18:46:22
TEST 2.3000E+11 HZ TEST.CVM.3
20
40
60
80
100
80
60
40
20
0
-20
-40
-60
ARC SEC
60
40
20
0
-20
-40
-60
-80
ARC SEC
Center at RA 00 00 0.000 DEC 10 00 0.00
Grey scale flux range= 0.3 109.5 JY/BEAM
Peak contour flux = 1.0951E+02 JY/BEAM
Levs = 1.0951E+00 * (4.000, 8.000, 16.00,
32.00, 64.00)

– Figure 5 –